UDC 621.313.39 https://doi.org/10.20998/2074-272X.2024.4.02

M.I. Kotsur

Development of methods for adapting the parameters of spatial end winding sections in 2D circuit-field models of induction-synchronous electric machines

Introduction. *Recently, the theory of a special class of cascade slow-speed non-contact induction-synchronous electrical machines (ISEM) has been developed. This allowed to obtain a combination of positive properties from conventional induction and synchronous electric machines.* ***Problem.*** *The lack of circuit and field models of ISEM imposes restrictions on further research of electromagnetic, mechanical and energy processes, in transient and quasi-steady modes of its operation.* ***Goal.*** *Development of 3D and adapted 2D circuit-field models of ISEM, decomposition methods, and dynamic synthesis with adaptation of electromagnetic parameter coupling conditions at the boundaries of calculated subdomains of ISEM.* ***Methodology.*** *Spatial elements of ISEM design are represented by separate spatial calculation subareas. The conditions of compliance with electromagnetic processes, which are formed by a complete calculation area and separate spatial calculation subareas of ISEM, are accepted. The influence of end effects and the parameters of the frontal parts of ISEM windings are determined by the inequality of the magnetic field energy of separate calculation subareas. These parameters, including end effects, are displayed as circuit elements in the 2D circuit-field model.* ***Results.*** *The obtained combination of 3D area decomposition methods and dynamic synthesis with adaptation of electromagnetic parameters coupling conditions at the boundaries of its calculated ISEM's subdomains. The proposed technique for determining the resistance and inductive resistances of the frontal parts of the ISEM windings, taking into account edge effects. The accuracy and effectiveness of the proposed methods is confirmed by the results of an experimental study.* ***Originality.*** *An adapted dynamic 2D circuit-field model of transient processes of ISEM has been developed, which allows taking into account parameters of the frontal parts of its windings.* ***Practical value.*** *The proposed methods can be used for various types of electrical machines.* References 27, tables 3, figures 12.

Key words: **electromagnetic field, end effects, methods of decomposition and dynamic synthesis, circuit-field modeling, electric machine.**

Вступ. *За останній час набули розвитку теорія спеціального класу каскадних тихохідних безконтактних асинхронно-синхронних електричних машин (АСЕМ) та отримана принципова нова її конструкція, за допомогою якої одержано поєднання позитивних властивостей від звичайних асинхронних та синхронних електричних машин.* ***Проблема.*** *Відсутність колових та польових моделей АСЕМ накладає обмеження щодо подальшого дослідження електромагнітних, механічних та енергетичних процесів, в перехідних та квазіусталеному режимах її роботи.* ***Мета.*** *Розробка 3D та адаптованої 2D коло-польових моделей АСЕМ, методів декомпозиції і динамічного синтезу з адаптацією умов сполучення електромагнітних параметрів на границях розрахованих підобластей АСЕМ.* ***Методологія.*** *Просторові елементи конструкції АСЕМ представляються просторовими окремими розрахунковими підобластями. Для кожній із цих підобластей ставиться у відповідність протікання електромагнітних процесів, які утворені цілісною розрахунковою областю. За нев'язкою енергії магнітного поля окремих підобластей з цілісною розрахунковою зоною визначаються дія крайових ефектів в торцевих зонах та параметри лобових частин обмоток АСЕМ. Ці параметри з врахуванням крайових ефектів відображаються як елементи кола для 2D коло-польової моделі АСЕМ.* ***Результати.*** *Отримана комбінація методів декомпозиції 3D області АСЕМ і динамічного синтезу з адаптацією умов сполучення електромагнітних параметрів на границях його розрахованих підобластей, яка дозволяє забезпечити чисельну реалізацію 3D коло-польового моделювання електромагнітних полів в окремих електричних та магнітних контурах складної просторової конструкції АСЕМ, а також визначити вплив крайових ефектів в торцевих зонах лобових частин АСЕМ за нев'язкою енергії магнітного поля. Запропонована методика щодо визначення активних та індуктивних опорів лобових частин обмоток АСЕМ з врахуванням дії крайових ефектів. Точність та ефективність запропонованих методів підтверджується результатами експериментального дослідження.* ***Наукова новизна.*** *Розроблена адаптована динамічна 2D коло-польова модель нестаціонарних взаємопов'язаних електромагнітних та електромеханічних процесів АСЕМ, яка дозволяє врахувати в перехідних режимах роботи параметри лобових частин його обмоток через її схемну реалізацію, нелінійність магнітних та електрофізичних властивостей активних матеріалів, поверхневі і крайові ефекти торцевих зон його активної частини.* ***Практична цінність.*** *Запропоновані методи можуть бути використані для різних типів електричних машин.* Бібл. 27, табл. 3, рис. 12.

Ключові слова: **електромагнітне поле, крайові ефекти, методи декомпозиції та динамічного синтезу, коло-польове моделювання, електрична машина.**

Introduction. Further improvement of designs and development of the theory of electric machines (EM) is directly related to the search for new technical solutions and technologies. This will enable the creation of devices with improved technical characteristics and high energy efficiency indicators of regulated electric drives, autonomous power supply systems for a number of consumers in industry, energy, agriculture, and special purpose devices.

Recently, the theory of a special class of cascade low-speed contactless induction-synchronous electric machines (ISEM) has been developed and a fundamentally new and improved design of it has been obtained [1]. This class of EM is a combination of two EMs, namely an induction motor (IM) and an inverted synchronous generator (SG) in a single magnetic core [2]. Here, the stator winding of the first EM is a three-phase $2p_1$-pole winding, and the stator winding of the second EM is a single-phase $2p_2$-pole excitation winding. The three-phase $2p_1$ winding and the single-phase $2p_2$ winding are electrically connected to each other and form a single conductive system on the stator (armature) side of the ISEM. The rotor combined winding is short-circuited with the number of mutually independent phase coils $n_2=p_1+p_2$ [3]. For this class of EM, various configurations of the combined stator winding with different variants of the ratio of the number of pairs of poles $2p_1/2p_2$ have been developed in [4], which makes it possible to obtain different values of the cascade synchronous speed of ISEM from 125 to 1000 rpm.

The latest improvement in the ISEM design puts this class of EM in terms of ease of manufacture and weight and size indicators in full compliance with classic induction EMs with a short-circuited rotor, with a control channel from the side of the fixed part of the ISEM armature. The simplicity of the design, the availability of control only from the side of the armature, the combination of IM and SG properties make this class of low-speed EM promising for further development. However, at present, for this class of EM, there is still no mathematical description and relevant research on electromagnetic and mechanical processes in the transient and quasi-steady modes of its operation, the control properties and characteristics of ISEM have not been determined. Therefore, in addition to conducting research on a physical sample of ISEM, there is a need to develop a mathematical model of ISEM, which will allow taking into account the design features and schematic implementation of the armature and rotor windings, as well as the nonlinearity of the magnetic and electrophysical properties of active materials, the skin and edge effects of the end zones of its active part, to obtain high accuracy and efficiency of the numerical implementation of electromagnetic parameters with a moderate use of computing resources, time consumption and stability of the computation process, with the reproduction of electromagnetic and mechanical processes as close as possible to the results of experimental research.

Analysis of research and publications. Modern methods of EM research are associated with the use of stationary and transient mathematical models of the transformation of electric, magnetic and mechanical energies [5]. Existing mathematical models of EM are divided into circuit and field models.

Circuit models are based on the theory of circuits and are based on the EM substitution circuits utilization. The interdependence between electric, magnetic, and design parameters of the EM is carried out between the inductive and active parameters of the EM substitution circuits [6]. Such models are described either by a system of algebraic equations or by a system of nonlinear differential equations of the first order. There are methods for designing and calculating the parameters of EM substitution circuits, which are based on empirical calculations and calculations based on catalog or experimental data [7]. In [8], the author states that in order to obtain a satisfactory accuracy of the numerical calculation of the parameters, the substitution circuits must be refined using field simulation. In [9], the methods of mathematical, structural and physical modeling in MATLAB of a DC motor with independent excitation and an induction motor with a short-circuited rotor were analyzed. The simulation results were compared with real experimental data. It was established that the disadvantage of this modeling method is the presence of a high calculation error, which is associated with the impossibility of fully taking into account all the features of the EM configuration, the nonlinearity of the electrophysical and magnetic properties of active materials.

The development of computer technology and specialized software complexes, such as ANSYS, COMSOL Multiphysics, OpenFEM, Impact, SALOME, Elmer, etc., has expanded the possibilities of practical use of 3D and 2D field modeling, which is based on the solution of a system of partial differential equations by the Finite Element Method [10]. In contrast to 2D field modeling, the application of 3D field modeling of electromagnetic processes can ensure the fulfillment of requirements for the accuracy of numerical calculations of electromagnetic parameters. For example, in [11] during the three-dimensional analysis of the magnetic field of a special spherical motor with permanent magnet with double stator, in [12] of a two-phase induction motor, in [13] of electromagnetic processes in the end zones of the rotor of a turbogenerator in its asymmetric modes of operation, the authors note an increase in the accuracy of the calculation in comparison with two-dimensional field modeling, which is confirmed by the results of an experimental study. However, depending on the problem to be solved, the authors use an assumption about the absence of frontal parts of the windings of their geometric EM models to reduce in the dimensionality of the problem itself. In [14], the analysis of the electromagnetic field in IM with short-circuited rotor is considered in the frequency and step-by-step time formulation of the problem for various 2D and 3D models of the rotor core destruction process and, at the end of this process, the core damage. The authors note the difficulty in implementing the 3D field modeling, reduce the convergence of numerical calculations at the boundary of two media with different magnetic and electrophysical properties, especially for complex nonlinear structural elements, significantly increase the calculation time and RAM requirements compared to 2D field modeling. Therefore, authors are proposed cases when the option of using a 2D model instead of a 3D model is accepted. In [15], the authors conducted an analysis of the distribution of the electromagnetic field along the EM, taking into account the complete design of the EM, that is, taking into account the frontal parts of its windings. It was established that in the end zones of the EM, the magnetic field energy increases in comparison with the value of the magnetic field energy in the active part, a comparative assessment of the calculation accuracy was carried out, depending on the choice of the degree of the Lagrange shape function when constructing the mesh of finite elements, the regularities of the increase in the calculation time were established, as well as RAM requirements. In [16], the authors performed an analysis of the numerical calculations of the EM based on its complete construction, an approach was proposed that would increase the finite elements using Lagrange shape functions of the first order within the boundaries of the calculation subdomains with different physical properties of the medium, which made it possible to increase the convergence of numerical calculations.

In most works related to the application of numerical field analysis, it is not necessary to take into account the frontal parts of the windings in the geometric model, which allows using 2D field modeling with sufficient accuracy. For example, in [17] the authors developed a method that allows, on the basis of a single approach, to calculate the geometric parameters of the frontal parts of the concentric and loop winding of the EM, taking into account their detailed structure and the sizes of all constituent elements, which gives much more accurate

results compared to classical methods of EM design. Also, in [18], a numerical field calculation and analysis of active and reactive resistances of IM windings in the entire range of changes in its slip was performed, with further calculation of its mechanical characteristics. However, taking into account the parameters of the frontal parts of EM windings using the methodology based on empirical equations is sufficient, provided that the system of phase currents is used as the initial conditions, taking into account the geometric direction of their flow. However, for cases when the distribution of currents in the conductive parts of the EM is unknown, especially when studying ISEM, both for 2D and for 3D field models of the EM, it is necessary to add circuit models to take into account the peculiarities of the circuit implementation of the connection of its windings.

In [19], the feasibility of using the circuit-field model of the EM, which is based on the combination of the 2D field model of the slot part of the EM with the circuit model of the stator winding of the EM, taking into account the schematic implementation of the connection of the coil groups of the phases of the stator windings of the EM, which makes it possible to additionally take into account parameters of their frontal parts is proved. As initial conditions, phase voltages are used when powered from a sinusoidal or non-sinusoidal source, which ensures the determination of currents in the process of numerical calculation. At the same time, it is possible to take into account the real-life distortion of the stator winding currents, which occurs even with a sinusoidal supply voltage.

Thus, taking into account the fact that the constant use of complex dynamic 3D circuit-field models, taking into account the schematic implementation of ISEM windings in the study of electromagnetic and mechanical processes in transient and quasi-steady modes of its operation, will lead to significant costs of computing resources, time and stability of the computational process, therefore there is a need to develop methods and approaches that will ensure the conditions of a qualitative transition from spatial to plane-parallel distribution of the electromagnetic field in the active part of ISEM while reducing the time spent on its numerical implementation and maintaining high accuracy of numerical calculation.

The goal of the work is the development of 3D and adapted 2D circuit-field models of ISEM, methods of decomposition and dynamic synthesis with adaptation of the conditions of coupling of electromagnetic parameters at the boundaries of the calculated subdomains of ISEM.

Object of study. Based on the MTF-111-6 crane motor (2.6 kW at duration of operation 100 %), an experimental sample of ISEM with cascade synchronous speed of rotation of the rotor n=500 rpm, U_n=127 V was made. The main dimensions of the experimental sample correspond to the MTF-111-6. The armature core has z_2=36 slots. The combined armature winding is three-phase-single-phase, two-layer with $2p_1$=4 and $2p_2$=8. The rotor core has z_2=30 slots, which are concentrated in 5 slots in a group. The number of slot groups is 6. Between the groups of ordinary slots, a massive toothed zone is formed, the number of which is equal to the number of slot groups. According to this, the groups of slots are placed at an angle of 60°, and the slots in the groups are respectively at an angle γ=6.66° (Fig. 1,*b*). The rotor winding has 6 phase short-circuited independent coils, 3 sections in each coil, which are placed around a massive tooth (Fig. 1,*b*).

3D circuit-field model of ISEM. The calculation 3D geometric model of ISEM accurately and in detail reflects the features of its design structure (Fig. 1), which includes the calculation subdomains of the components of its active part: armature core 1; three-phase-single-phase $2p_1$=4 and $2p_2$=8 armature winding 2; insulation system in the slot zone of the armature core 3; rotor core 4; independent short-circuited rotor winding 5; insulation system in the slot zone of the rotor core 6 (Fig. 1,*b*). The coil sections of the armature winding consist of frontal and slot parts, which are connected geometrically and form 12 coils, 2 coils in each coil group (two coil groups per phase). The coils of the armature and rotor windings have complete geometric symmetry between them. Each coil of the armature winding has input 7 and output 8 (Fig. 1,*a*). The rotor winding consists of 6 independent phase coils A, B, C, D, E, F (Fig. 1,*b*). Each phase coil contains 3 sections – 1, 2, 3 (Fig. 1,*b*), which are connected together in a short circuit.

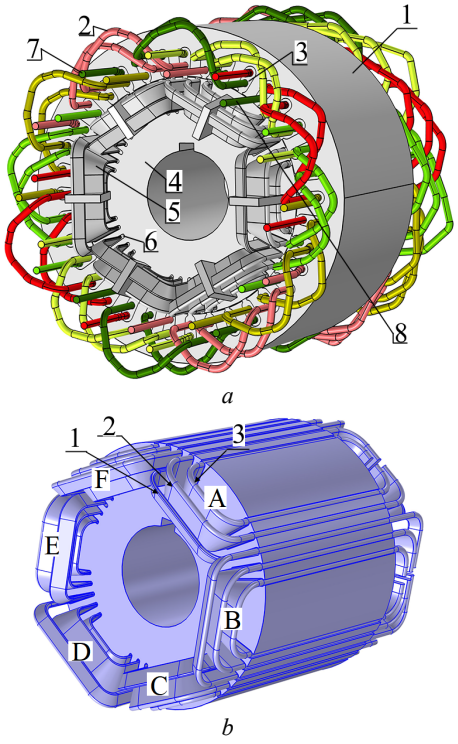

Fig. 1. Complete 3D geometric model of ISEM (*a*); calculation 3D geometric model of ISEM rotor (*b*)

The mathematical description of electromagnetic processes assumes the isotropic nature of the electrophysical and electromagnetic properties of materials, the absence of displacement currents and free charges [20]. In this case, the transient electromagnetic processes in ISEM in the short-circuit mode can be described by a coupled system of nonlinear partial differential equations [21]:

$$\begin{cases} \sigma_j \partial \boldsymbol{A}_j / \partial t + \sigma_j(\theta_j)\nabla V_j + \nabla \times \left[\left(\mu_0 \mu_j(B) \right)^{-1} \nabla \times \boldsymbol{A}_j \right] = \boldsymbol{J}_{ej}; \\ -\nabla \cdot \partial\left(\varepsilon_0 \varepsilon_r \nabla V_j \right) / \partial t - \nabla \cdot \left(\sigma_j(\theta_j) \cdot \nabla V_j - \boldsymbol{J}_{ej} \right) = 0, \end{cases} \quad (1)$$

where $\boldsymbol{A}$ is the magnetic vector potential; V is the electric scalar potential; $\boldsymbol{B}$ is the magnetic flux density; μ, ε_r, $\sigma(\theta)$ ate, respectively, the relative magnetic and dielectric permeability, specific electrical conductivity (for each calculation domain it is specified separately according to the magnetic, electrophysical and dielectric properties of materials); θ is the temperature; ω is the angular frequency; $\boldsymbol{J}_e$ is the density of the external current source; subscripts j correspond to subdomains of the geometric calculation domain. In accordance with [20, 21], the system of equations (1) is supplemented by the Coulomb gauge condition div($\boldsymbol{A}$)=0.

Uniform boundary conditions are set on the outer boundaries of the 3D domain of the generalized ISEM geometric model [21]:

$$\begin{cases} \boldsymbol{A}_j = 0\big|_{\forall j\in(1,6)},\ A_j = \overline{k}\cdot A_y(x,z)\big|_{j=1}, \\ V_j = \varphi_j\big|_{\forall j\in(2,6)}, \\ \boldsymbol{n}_j\cdot\left(\boldsymbol{J}_j\right)=0\big|_{j=1} \end{cases} \tag{2}$$

and coupling conditions for magnetic and electric fields:

$$\begin{cases} \boldsymbol{n}_{i,k}\times\left(\boldsymbol{H}_i-\boldsymbol{H}_k\right)=0\big|_{\forall i,k\in(1,6),i\neq k}, \\ \boldsymbol{H}=\left(\mu_0\mu\right)^{-1}\nabla\times\boldsymbol{A}, \\ \boldsymbol{n}_{i,k}\cdot\left(\boldsymbol{J}_i-\boldsymbol{J}_k\right)=0\big|_{\forall i,k\in(1,6),i\neq k}, \\ \boldsymbol{J}=\sigma(\theta)\cdot\boldsymbol{E},\ \boldsymbol{E}=-\nabla V-\partial\boldsymbol{A}/\partial t, \end{cases} \tag{3}$$

where $\boldsymbol{H}$ is the magnetic field strength; $\boldsymbol{E}$ is the electric field strength.

The design of the two-layer three-phase-single-phase combined winding of the ISEM armature contains 2 coil groups (2 coils in each coil group) per phase. The first and third, second and fourth coils are connected in series. The second and fourth coils are connected in parallel with the first and third coils. The outputs of the coil groups of all phases are connected in two independent «stars» – zero points «0+» and «0–» (Fig. 2). Regarding the inputs of phases A, B, C, to which the alternating voltage is supplied, the combined armature winding of ISEM is a conventional three-phase winding with the number of pole pairs $2p_1$=4. Relative to the zero points «0+» and «0–», to which the constant voltage is supplied, it is single-phase, with the number of pairs of poles $2p_2$=8.

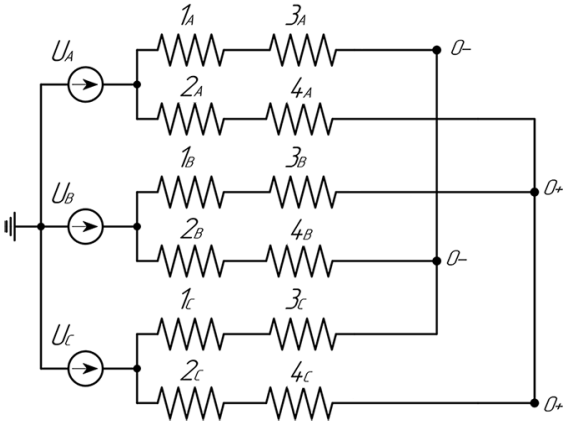

Fig. 2. Electrical diagram of the model implementation of power supply of coil groups of phase windings of the ISEM armature

When studying the processes of electromagnetic energy conversion in ISEM, it is assumed that it is connected to a network with unlimited power and a symmetrical system of phase voltages [21]. Therefore, the initial conditions correspond to the first commutation law [21]:

$$\begin{cases} i_A\big|_{0-}=i_A\big|_{0+}=0; \\ i_B\big|_{0-}=i_B\big|_{0+}=0; \\ i_C\big|_{0-}=i_C\big|_{0+}=0, \\ u_A(t)=\sqrt{2}\cdot U_{fase}\cdot\sin(\omega\cdot t); \\ u_B(t)=\sqrt{2}\cdot U_{fase}\cdot\sin(\omega\cdot t+2\pi/3); \\ u_C(t)=\sqrt{2}\cdot U_{fase}\cdot\sin(\omega\cdot t-2\pi/3). \end{cases} \tag{4}$$

The geometric model of the ISEM armature winding coil (Fig. 1) is implemented in the form of one effective conductor. The number of turns of the ISEM armature winding coils is taken into account according to the equation [21]:

$$\boldsymbol{J}_e=\frac{n\cdot I_{cir}}{S_{cir}}\boldsymbol{e}_{coil}, \tag{5}$$

where n is the number of winding turns; I_{cir} is the phase current; S_{cir} is the cross section of the effective conductor; $\boldsymbol{e}_{coil}$ is the vector variable representing the local density of effective conductors in the coil, length and cross section.

The schematic implementation of the armature winding (Fig. 2) together with the equations of the mathematical model of the electromagnetic field can be performed, for example, with the help of COMSOL Multiphysics using the multiphysics structure when combining the «Rotating Machinery, Magnetic» and «Electrical Circuit» interfaces. The connection and agreement of the parameters of the armature winding, which are elements of both the field model and the elements of the electric circuit, is performed with the help of «External I vs. U» terminals. A schematic implementation for the ISEM rotor winding is not required, since the connection of sections to each other for each of the phase coils of the rotor winding is implemented geometrically.

Decomposition and dynamic synthesis methods for modeling complex spatial elements of the active part of ISEM. The application of 3D field modeling of transient electromagnetic processes in ISEM, taking into account the multi-component spatial structure, as well as the nonlinearity of the electrophysical and magnetic properties of active materials, allows to reproduce with high accuracy and efficiency the peculiarities of the flow of transient electromagnetic processes. However, when taking into account the rotation of the moving part of the active part of the ISEM, that is, the rotor itself, difficulties arise in the numerical implementation of the problem of calculating the 3D transient electromagnetic field, which is associated with an increase in the degree of freedom of the electromechanical system, namely, an increase in the number of independent variables in the general system of equations, which requires significant increase in computing resources. Therefore, it is expedient to switch to the plane-parallel formulation of the ISEM electromagnetic field with the implementation of rotor

rotation. This requires the development of special approaches for 3D modeling of electromagnetic fields, which will allow for the coordination of field and circuit models of ISEM.

The mathematical procedure of decomposition of a complex electrotechnical system of ISEM consists in the representation of the spatial calculation domain by several separate subdomains – calculation zones. Each of these zones should be matched with the flow of electromagnetic processes, which are formed by a complete calculation domain. The purpose of the decomposition of a complex ISEM electrotechnical system is to separate the frontal parts of the armature and rotor windings from the spatial model of the ISEM and display them in the schematic model while preserving the connections of electromagnetic processes between them, which will allow us to obtain grounds for an adaptive transition to plane-parallel circuit-field modeling.

The ISEM spatial calculation domain (Fig. 1) can be divided into 6 separate calculation subdomains (Fig. 3): *a* – core and slot part of the ISEM armature winding (*j*=1), *b* – respectively, left (*j*=2) and right (*j* =3) front parts of the armature winding; *c* – core and slot part of the rotor winding (*j*=4); *d* – respectively, left (*j*=5) and right (*j*=6) front parts of the phase coils of the rotor winding.

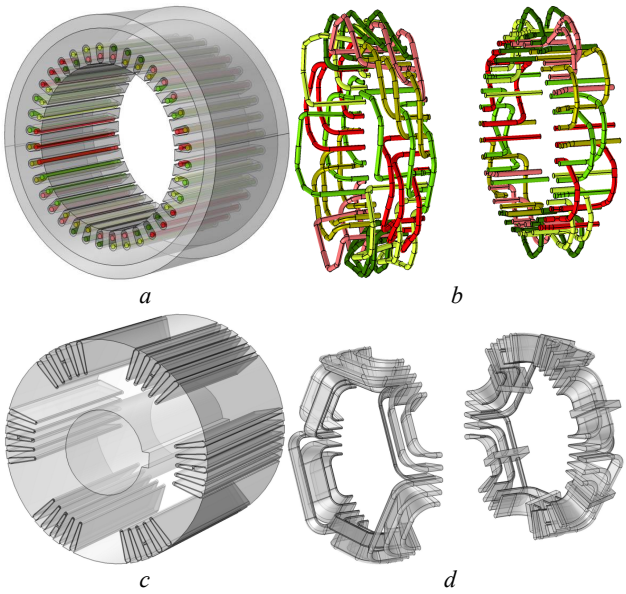

Fig. 3. Decomposition 3D ISEM calculation zones:
the core and slot part of the armature winding (*a*);
left and right front parts of the armature winding (*b*);
core and slot part of the rotor winding (*c*);
left and right front parts of the phase coils of the rotor winding (*d*)

Then, in integral relations, the volume of the area of electromagnetic energy conversion of alternating and direct currents for ISEM can be represented as the sum of the volumes of the above-mentioned six subdomains:

$$\iiint_{V} \mathrm{d}x\mathrm{d}y\mathrm{d}z = \sum_{i=1}^{6} \iiint_{V_i} \mathrm{d}x\mathrm{d}y\mathrm{d}z\,. \qquad (6)$$

In this case, electrical losses and magnetic energy in the domain of the active part of the ISEM are defined as the sum of their values for the corresponding subdomains in the form:

$$P_{\Sigma} = \sum_{i=1}^{6} P_i = \sum_{i=1}^{6} \iiint_{V_i} \sigma_{i,j}(\theta)^{-1} \left|\dot{\boldsymbol{J}}_i\right|^2 \mathrm{d}x\mathrm{d}y\mathrm{d}z, \qquad (7)$$

$$W_{\Sigma} = \sum_{i=1}^{6} W_i = \sum_{i=1}^{6} \iiint_{V_{i,j}} \mu_i \mu_0 \left(\dot{\boldsymbol{H}}_i, \dot{\boldsymbol{H}}_i\right) \mathrm{d}x\mathrm{d}y\mathrm{d}z. \qquad (8)$$

When decomposing the three-dimensional domain of the active part of ISEM in the zones that form it, electromagnetic processes are described by differential equations (1) with conditions (2), (3), but they can be considered separately from each other. At the same time, appropriate conditions must be set at the boundaries of their connection.

For the slot zone of the armature core and the rotor, the plane-parallel field conditions are set:

$$\left\{ n \times \boldsymbol{H} = 0 \right|_{\Omega_{i,i+1}}. \qquad (9)$$

At the junction of the surfaces of the frontal and slot parts of the armature and rotor windings, the following conditions are accepted:

$$A_{z,i} = A_{z,i+1}\big|_{\Omega_{i,i+1}}, \qquad (10)$$

$$A_{x,i} = A_{y,i} = 0\big|_{\Omega_{i,i+1}}. \qquad (11)$$

Also, the condition of equality of electric potentials is assumed at the junction of the surfaces of the frontal and slot parts of the armature winding:

$$\left\{U_i = U_{i+1}\right\}\big|_{\Omega_{i,i+1}} = \mathrm{const}_j, \qquad (12)$$

as well as the condition of equality of currents for the sections of the phase short-circuited coils of the rotor winding:

$$\left\{I_{rm} = I_{rm+1}\right\}\big|_{\Omega_{m,m+1}} = \mathrm{const}_n. \qquad (13)$$

The currents in the coil groups of the armature winding are determined for the given values of the short-circuit voltage U_{sc}:

$$\Delta\dot{\boldsymbol{U}}_{sc} = \sum_{i} \left\{\Delta\dot{\boldsymbol{U}}_{i,j}\right\}, \qquad (14)$$

where $\left\{\Delta\dot{\boldsymbol{U}}_{i,j}\right\}$ is the voltage drop; *i*, *j* are the number of series and parallel branches of the armature winding.

In conjunction conditions (14), const_i values are «free». Therefore, the potential at the outer boundaries of the conjugation of the subdomains of the frontal and slot parts of the armature winding, as well as the values of the currents at the boundaries of the conjugation of the slot and frontal parts of the sections of the phase coils of the rotor winding cannot be specified in advance. They are determined from the solution of the optimization problem.

Therefore, when synthesizing calculation zones in the 3D domain of the contour, the synthesis accuracy criterion and the corresponding objective function are determined by the sum of the squares of residuals of the current amplitudes in the armature and ISEM rotor windings:

$$\min\left\{ M(\boldsymbol{D},\boldsymbol{R}) = \sum_{j} \Delta\dot{\boldsymbol{I}}^2_{\Sigma j} = \sum_{j} \left(\sum_{i} \dot{\boldsymbol{I}}_i - \dot{\boldsymbol{I}}_{sc} \right)^2_j \right\}. \qquad (15)$$

In the general case, the objective function $M(\boldsymbol{D},\boldsymbol{R})$ is a function of vectors of independently varied $\boldsymbol{D}$ and

dependent $\boldsymbol{R}$ parameters. The voltage drops on the sections of the armature winding contours are considered as projections of the vector of independently varied parameters $\boldsymbol{D}$. This makes it possible to transform the objective function $M(\boldsymbol{D},\boldsymbol{R})$ into the function $\tilde{M}(\boldsymbol{D})$ and bring the optimality condition (15) to the form:

$$\min \tilde{M}(\boldsymbol{D}) = \sum_j \left(\sum_i \dot{\boldsymbol{I}}_i(\boldsymbol{D}) - \dot{\boldsymbol{I}}_{sc} \right)_j^2 . \qquad (16)$$

To implement task (16), it is advisable to apply the well-proven method of dynamic programming [22] for a similar class of tasks.

When constructing a recurrent system of Bellman equations the vector of optimization parameters with components $\Delta\dot{\boldsymbol{U}}_{i,j}$ should be represented as a sum of initial approximation vectors [22]:

$$\left\{\Delta\dot{\boldsymbol{U}}_{i,j}\right\} = \left\{\Delta\dot{\boldsymbol{U}}_{i,j}\right\}_0 + \left\{\delta\Delta\dot{\boldsymbol{U}}_{i,j}\right\}_1 . \qquad (17)$$

This will allow representing the objective function as:

$$\tilde{M}\left(\left\{\Delta\dot{\boldsymbol{U}}_{i,j}\right\}\right) = \tilde{M}\left(\left\{\Delta\dot{\boldsymbol{U}}_{i,j}\right\}_0 + \left\{\delta\Delta\dot{\boldsymbol{U}}_{i,j}\right\}_1\right) = \\ = \tilde{M}_0 + \Delta\tilde{M}\left(\boldsymbol{D}_0, \boldsymbol{\delta D}_1\right) = \tilde{M}_0 + \Delta\tilde{M}_1. \qquad (18)$$

Let us represent the optimality condition (16) as a system of recurrent Bellman equations [22]:

$$\min \Delta\tilde{M}_\Sigma = \Phi(\boldsymbol{D}_0) = \min_{\boldsymbol{\delta D}_1} \ldots \min_{\boldsymbol{\delta D}_k} \left[\left(\Delta\tilde{M}_1(\boldsymbol{D}_0, \boldsymbol{\delta D}_1) + \ldots \right. \right. \\ \left. \left. \ldots + \Delta\tilde{M}_k(\boldsymbol{D}_{k-1}, \boldsymbol{\delta D}_k) \right) \right] \qquad (19)$$

Relationships (16) and (19) determine the dynamic adaptation of electromagnetic field coupling conditions (9) – (14) between the frontal part of the calculation zone and the active part of the slot of 3D calculation zone of the ISEM armature and rotor. The iterative computation process is implemented by means of dynamic programming [22] with specified accuracy of current amplitude modulus $\varepsilon_I \le 0.1$ % and phases $\varepsilon_\varphi \le 0.5$ %. For direct current, accuracy is specified only in absolute value.

Figures 4, 5 show the results of field modeling of the decomposed calculation zones of the active part of ISEM in the form of the distribution of the z-component of the magnetic vector potential A_z and the magnetic field energy E using the method of dynamic adaptation according to the criterion of current errors. The results of the numerical calculation were compared with the results obtained for a complete calculation zone, both for the ISEM field model (Fig. 1,*a*) and with separate field model of the active part of the ISEM armature [21]. Table 1 shows the errors of calculations by the method of dynamic adaptation of field models during the synthesis of the electromagnetic circuit of the decomposed zones of the active part of ISEM. Here, discrepancy for active losses power is 0.042 – 0.109 % for alternating current, and 0.015 – 0.0184 % for direct current, depending on the calculated subdomain of the structural elements of the active part of the ISEM.

Discrepancy by voltage drop in the frontal and slot parts of the armature winding is 0.74 – 0.98 % (for alternating current) and 0.0211 – 0.091 % (for direct current), respectively.

Based on the results of the numerical calculation, the components of the magnetic field energy of the decomposed zones of the active part of the ISEM armature were determined, and the discrepancy between the total value of the magnetic field energy and the value of the magnetic field energy in the numerical calculation of the integral calculation zone of the active part of the armature was calculated (Table 1). Since the energy of the magnetic field is a dependent parameter during the optimization of individual calculation zones when applying (15), the significant discrepancy in the value of the magnetic field energy for alternating current $\delta E_a|_{AC}$ = 14.841 % and for direct current $\delta E_a|_{DC}$ = 4.587 % is caused by not taken into account the action of edge effects, which leads to magnetization by the frontal parts of the winding in the end zone of the armature core. To take into account the effect of edge effects for numerical calculation problems with separate 3D zones for the optimization equation (15), the magnetic field energy parameter must be assigned to the group of varied parameters $\boldsymbol{D}$. At the same time, the error in the magnetic field energy will be reduced by alternating current to $\delta E_a|_{AC}$ = 0.274 % and by direct current up to $\delta E_a|_{DC}$ = 0.0831 %.

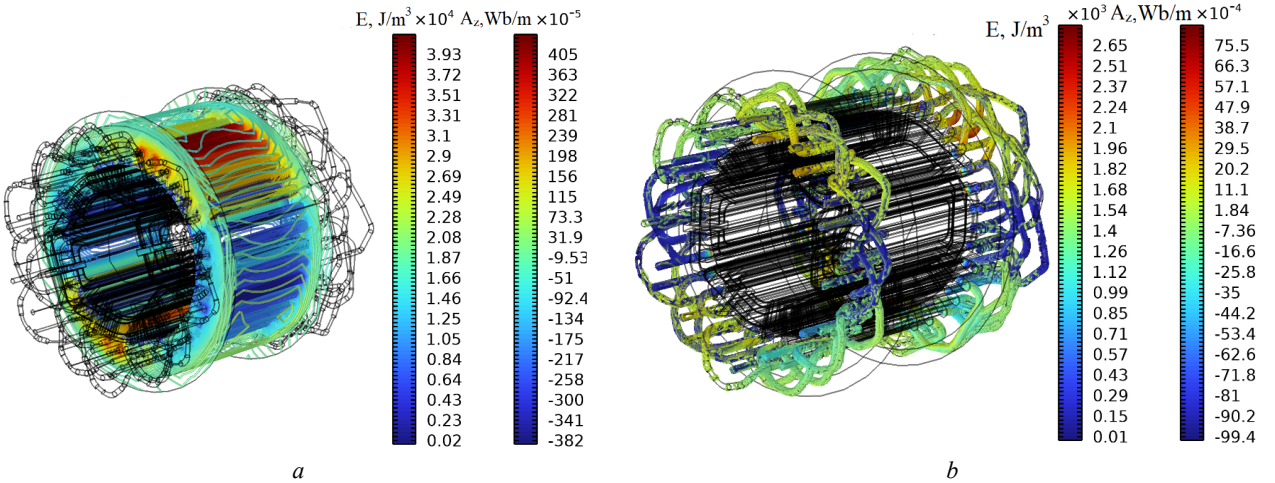

a *b*

Fig. 4. z-component of the magnetic vector potential A_z and the energy of the magnetic field E in the active part of the ISEM armature: *a* – slot zone of the active part of the armature (j = 1); *b* – the frontal zone of the active part of the armature (j = 2,3)

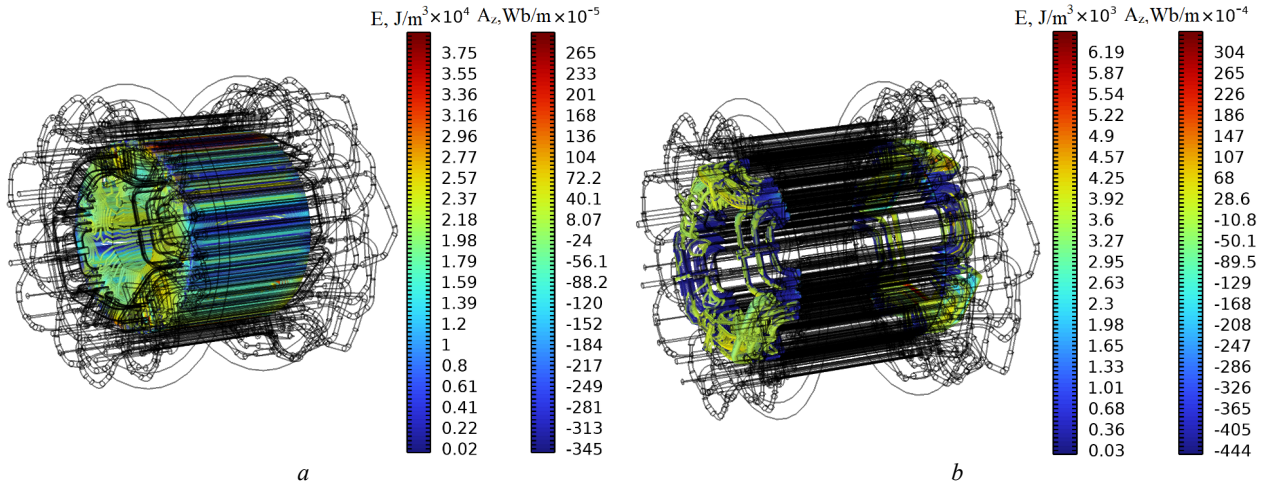

a *b*

Fig. 5. *z*-component of the magnetic potential vector A_z and the magnetic field energy E in the active part of the ISEM rotor: *a* – slot zone of the active part of the rotor (j = 4); *b* – the frontal zone of the active part of the rotor (j = 5,6)

Table 1

Calculation errors by the method of dynamic adaptation of field models in the synthesis of an electromagnetic circuit of decomposed zones of the active part of ISEM

Calculation subdomains (zones)	slot zone of the active part of the armature (j=1)	frontal zone of the active part of the armature (j=2,3)	slot zone of the active part of the rotor (j=4)	frontal zone of the active part of the rotor (j=5,6)
Losses of active power (from alternating / direct currents)	0,042 % / 0,015 %	0,064 % / 0,0168 %	0,096 % / 0,019 %	0,109 % / 0,0184 %
Voltage drop (module / phase)	0,74 % / 0,091 %	0,98 % / 0,0211 %	–	–
DC voltage drop	0,184 %	0,156 %	–	–
Energy of the magnetic field of the active part of the armature	when modeling the active part of the armature (when separating the active part of the rotor) (from AC/DC currents)			
	$\delta E_a\|_{AC/DC}$ = 14,841 % / 4,587 %			
Energy of the magnetic field of the active part of the rotor	when modeling the active part of ISEM (when separating the active part of the rotor) (from AC/DC currents)			
	$\delta E_r\|_{AC/DC}$ = 6,33 % / 1,71 %			

In another case, for the tasks of replacing the spatial elements of the front parts of the armature winding with elements of an electric circuit (in the tasks of adapting 3D to 2D numerical calculations), the effect of edge effects, in relation to magnetization by the front parts, can be taken into account through the addition of mutual inductance between the slot and front zones of the armature winding, which can be determined using the following expression, according to [21]:

$$L_j\Big| = 2 \cdot W_j \Big/ I_j{}^2 . \qquad (20)$$

At the same time, the energy of the magnetic field, which reflects the manifestation of the edge effect, can be defined as:

$$E\big|_{end.a} = E_{res}\big|_a - \left(\sum_{j=1}^{3} E_j \right), \qquad (21)$$

where E_j is the energy of the magnetic field of the j-th calculation subdomain; $E_{res}|_a$ is the energy of the magnetic field when modeling the active part of the armature (when separating the active part of the rotor).

By the same method, it is possible to determine the mutual inductance between the slot and frontal zones of the sections of the phase coils of the rotor winding. At the same time, the energy of the magnetic field, which reflects the effect of magnetization of the frontal zone in the end region of the rotor core, can be defined as:

$$E\big|_{end.r} = E_{res}\big|_{em} - E_{res}\big|_a - \left(\sum_{j=4}^{6} E_j \right), \qquad (22)$$

where $E_{res}|_{em}$ is the energy of the magnetic field when simulating the active part of ISEM.

Thus, the reliability and accuracy of modeling results using methods of decomposition of 3D active part zone of the ISEM and dynamic synthesis of electrical parameters in its circuit can be ensured provided that the distribution of electric potentials on the boundaries of the connection of zones is close to uniform, and the distribution of the magnetic field corresponds to a plane-parallel field. In this case, the sum of active losses and energy of the magnetic field, taking into account edge effects in the area of conjugation of slot and frontal parts in the calculation zones, will correspond with high accuracy to active losses and magnetic energy losses for the 3D domain of the entire active part of ISEM.

Determination of active resistances and inductances of end parts of windings when modeling complex spatial elements of the active part of ISEM. In the case when the speed of rotation of the rotor $n > 0$, the active resistance and total inductance of the rotor winding will depend on the rotor slip s of ISEM. Therefore, for the adaptive transition from 3D to plane-parallel circuit-field modeling, it is necessary to additionally take into account the change in active resistance and inductance of the frontal parts of the sections of the phase coils of the rotor

winding in the form of dependencies $R^{end}{}_r=f(s)$ and $L^{end}{}_r=f(s)$. To do this, for the calculation domain of the frontal parts of the armature windings and the ISEM rotor, we will use the variational formulation of the electromagnetic field equations (1) [23], which allows us to set the equation of rotation of the electromagnetic field in the calculation domain of the frontal part of the rotor winding coils relative to the stationary magnetic field of the calculation domain of the frontal part of the armature winding. In this case, when solving the boundary value problem for the first equation of the system of equations (1), it is necessary to multiply the left and right parts by the trial vector function $\boldsymbol{\psi}$ from the space of trial functions H^{rot} on the boundaries of the inner S_0 and outer S_1 surfaces Ω of the frontal part of the rotor winding (upon fulfillment of the condition $\boldsymbol{n}\times\boldsymbol{\psi}=0$) and must be integrated over the volume of the calculation domain Ω:

$$\iiint_V \boldsymbol{\psi}\cdot\left[\nabla\times\left(\mu_0^{-1}\mu_r^{-1}\nabla\times\boldsymbol{A}\right)\right]\mathrm{d}x\mathrm{d}y\mathrm{d}z+\ldots$$
$$\ldots+\iiint_V \boldsymbol{\psi}\cdot\left(j\sigma\omega\boldsymbol{A}+\sigma\nabla V\right)\mathrm{d}x\mathrm{d}y\mathrm{d}z=\iiint_V \boldsymbol{\psi}\cdot\boldsymbol{J}_e\mathrm{d}x\mathrm{d}y\mathrm{d}z. \quad (23)$$

To reduce the order of differentiation in the integrand expression of the first volume integral, it is necessary to use the relation for the *curl* operator

$$\boldsymbol{v}\cdot\nabla\times\boldsymbol{u}-\boldsymbol{u}\cdot\nabla\times\boldsymbol{v}=\nabla\cdot\left(\boldsymbol{u}\times\boldsymbol{v}\right).$$

Let's accept that

$$\boldsymbol{v}=\boldsymbol{\psi},\quad \boldsymbol{u}=\mu\nabla\times\boldsymbol{A},\ \text{and}\ \ \mu=\mu_0^{-1}\mu_r^{-1},$$

then the relation (23) will have the form:

$$\iiint_V \mu\cdot\left(\nabla\times\boldsymbol{A}\right)\left(\nabla\times\boldsymbol{\psi}\right)\mathrm{d}x\mathrm{d}y\mathrm{d}z+\ldots$$
$$\ldots+\iiint_V \nabla\cdot\left[\left(\mu\nabla\times\boldsymbol{A}\right)\times\boldsymbol{\psi}\right]\mathrm{d}x\mathrm{d}y\mathrm{d}z+\ldots \quad (24)$$
$$\ldots+\iiint_V \boldsymbol{\psi}\cdot\left(j\sigma\omega\boldsymbol{A}+\sigma\nabla V-\boldsymbol{J}_e\right)\mathrm{d}x\mathrm{d}y\mathrm{d}z=0.$$

Next, we convert the second volume integral into a surface integral using the Gauss–Ostrogradsky formula [24]:

$$\iiint_V \nabla\cdot\left(\boldsymbol{u}\right)\mathrm{d}x\mathrm{d}y\mathrm{d}z=\iint_S \boldsymbol{u}\cdot\boldsymbol{n}\mathrm{d}S,$$

taking into account that

$$\boldsymbol{u}=\left(\mu\nabla\times\boldsymbol{A}\right)\times\boldsymbol{\psi},$$

and

$$\left(\boldsymbol{u}\times\boldsymbol{v}\right)\cdot\boldsymbol{w}=-\left(\boldsymbol{w}\times\boldsymbol{v}\right)\cdot\boldsymbol{u}.$$

Then equation (24) can be represented as:

$$\iiint_V \mu\cdot\left(\nabla\times\boldsymbol{A}\right)\left(\nabla\times\boldsymbol{\psi}\right)\mathrm{d}x\mathrm{d}y\mathrm{d}z-\iint_S\left(\boldsymbol{n}\times\boldsymbol{\psi}\right)\left(\mu\nabla\times\boldsymbol{A}\right)\mathrm{d}S+\ldots$$
$$\ldots+\iiint_V \boldsymbol{\psi}\cdot\left(j\sigma\omega\boldsymbol{A}+\sigma\nabla V-\boldsymbol{J}_e\right)\mathrm{d}x\mathrm{d}y\mathrm{d}z=0. \quad (25)$$

Since only the boundary condition of the first kind, for which $\boldsymbol{n}\times\boldsymbol{\psi}=0$, is set on the surfaces S_0 and S_1, which limit the calculated domain of the frontal parts of the phase coils of the rotor winding Ω, then for equation (25) in its final form it can be represented as:

$$\iiint_V \mu\cdot\left(\nabla\times\boldsymbol{A}\right)\left(\nabla\times\boldsymbol{\psi}\right)\mathrm{d}x\mathrm{d}y\mathrm{d}z+\ldots$$
$$\ldots+\iiint_V \boldsymbol{\psi}\cdot\left(j\sigma\omega\boldsymbol{A}+\sigma\nabla V-\boldsymbol{J}_e\right)\mathrm{d}x\mathrm{d}y\mathrm{d}z=0. \quad (26)$$

We multiply the second equation from the system of equations (1) by the function N from the space of trial scalar functions Φ with simultaneous integration over the volume V [24]:

$$-\iiint_V N\cdot\left[\nabla\cdot\left(j\sigma\omega\boldsymbol{A}+\sigma\nabla V-\boldsymbol{J}_e\right)\right]\mathrm{d}x\mathrm{d}y\mathrm{d}z=0. \quad (27)$$

To reduce the order of differentiation, we will use the relation for the divergence operator

$$\nabla\cdot\left(f\boldsymbol{u}\right)=f\,\nabla\cdot\boldsymbol{u}+\boldsymbol{u}\nabla f.$$

If we make the assumption that

$$f=N,\quad \boldsymbol{u}=\boldsymbol{J},$$

where the total current can be defined as [26]:

$$\boldsymbol{J}=\sigma\nabla V+j\sigma\omega\boldsymbol{A}-\boldsymbol{J}_e, \quad (28)$$

then according to (27) we get that

$$\iiint_V\left(\boldsymbol{J}\cdot\nabla N\right)\mathrm{d}x\mathrm{d}y\mathrm{d}z-\iiint_V\nabla\cdot\left(N\boldsymbol{J}\right)\mathrm{d}x\mathrm{d}y\mathrm{d}z=0. \quad (29)$$

Let's transform the second volume integral into a surface integral, and make the assumption that

$$\boldsymbol{u}=N\cdot\boldsymbol{J},$$

then:

$$\iiint_V\left(\boldsymbol{J}\cdot\nabla N\right)\mathrm{d}x\mathrm{d}y\mathrm{d}z-\iint_S\left(N\boldsymbol{J}\cdot\boldsymbol{n}\right)\mathrm{d}x\mathrm{d}y=0. \quad (30)$$

In its final form, the equivalent variation formulation for equations (1) will have the form:

$$\begin{cases}\iiint_V \mu\left(\nabla\times\boldsymbol{A}\right)\left(\nabla\times\boldsymbol{\Psi}\right)\mathrm{d}x\mathrm{d}y\mathrm{d}z+\iiint_V\left(\boldsymbol{J}\cdot\boldsymbol{\Psi}\right)\mathrm{d}x\mathrm{d}y\mathrm{d}z=0;\\ \iiint_V\left(\boldsymbol{J}\cdot\nabla N\right)\mathrm{d}x\mathrm{d}y\mathrm{d}z-\iint_{S_1}\left(NJ_n\right)\mathrm{d}x\mathrm{d}y=0.\end{cases} \quad (31)$$

To solve the variational equation (31), the sought scalar potential V is represented in the form of expansion by quadratic Lagrangian basis functions, and the magnetic vector potential by second-order basis vector functions. Figure 6 shows the results of the numerical calculation in the form of lines of force of the magnetic vector potential, as well as x-, y-, z-components of the magnetic vector potential A_x, A_y, A_z for the calculation domain of the frontal parts of the armature windings and the ISEM rotor.

Based on the found distribution of potential $\boldsymbol{A}$, full current $\boldsymbol{J}$ and electric field strength $\boldsymbol{E}$, it is possible to find the active resistance and inductance of the frontal parts of the sections of the phase coils of the rotor winding, taking into account the speed of rotation of the electromagnetic field relative to the frontal parts of the ISEM armature winding [25]:

$$\begin{cases}R=\dfrac{\iiint_V \mathrm{Re}\left(\boldsymbol{J}\cdot\boldsymbol{E}^*\right)\mathrm{d}x\mathrm{d}y\mathrm{d}z}{\left|I_i\right|^2};\\ L=\dfrac{1}{I_i{}^2}\iiint_V\left(\boldsymbol{A}\cdot\boldsymbol{J}^*\right)\mathrm{d}x\mathrm{d}y\mathrm{d}z,\end{cases} \quad (32)$$

where I_i is the current in the i-th circuit of the calculation domain; E^*, J^* are the complex-conjugate quantities of electric field strength and full current, respectively.

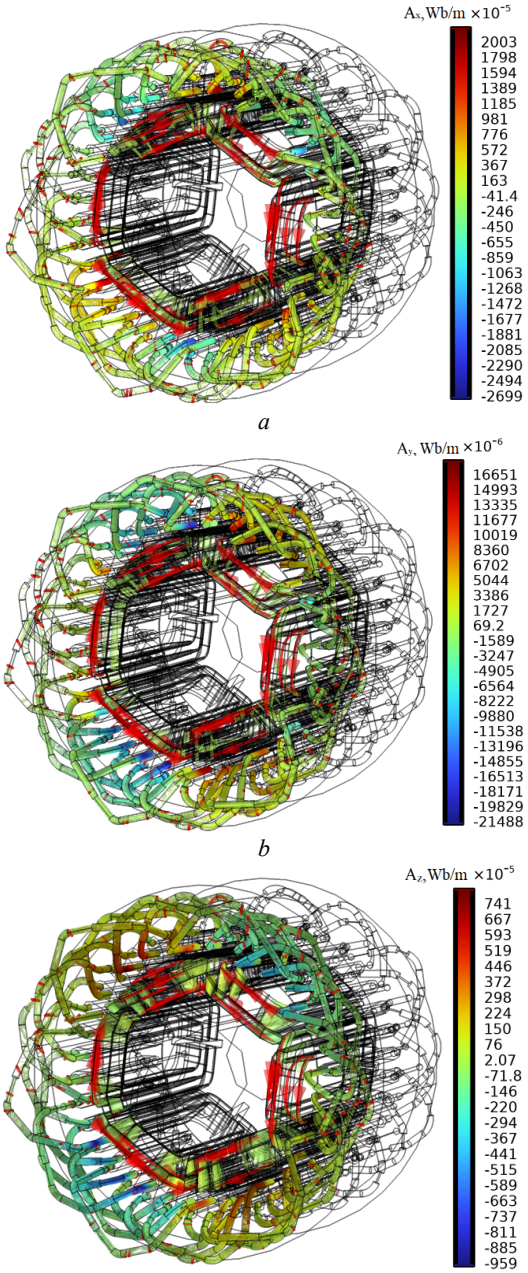

Fig. 6. Components A_x (*a*), A_y (*b*), A_z (*c*) of the magnetic vector potential in the domain of the front parts of the armature windings and ISEM rotor

Inductance and mutual inductance of the front parts of the armature winding:

$$L_{ii} \vee L_{jj} = \frac{1}{I^2_{i\vee j}} \left(\iiint_V (\boldsymbol{A} \cdot \boldsymbol{J}) \mathrm{d}x\mathrm{d}y\mathrm{d}z \right) \Bigg|_{I_{i\vee j}=0}, \quad (33)$$

$$M_{ij} = \frac{1}{I_i \cdot I_j} \left(\iiint_V (\boldsymbol{A} \cdot \boldsymbol{J}) \mathrm{d}x\mathrm{d}y\mathrm{d}z - L_{ii} \cdot I_i^2 \right) \Bigg|_{I_{i\wedge j\neq 0}}, \quad (34)$$

where I_i, I_j are the currents in i and j phases of the armature winding.

If during the rotation of the front parts of the rotor windings, the total inductance of the front parts of the armature winding L_i does not change, that is, its value corresponds to the value when the front parts of the rotor winding are statically placed relative to the armature, then the total inductance and active resistance of the front parts of the rotor winding will depend on the sliding of the ISEM rotor (Fig. 7).

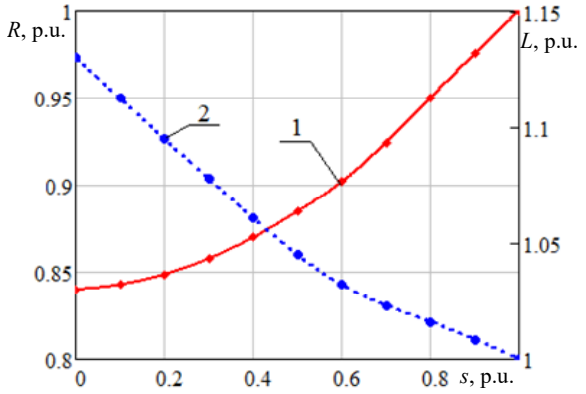

Fig. 7. Results of the numerical calculation regarding the dependence of the active resistance (1) and total inductance (2) of the front parts of the sections of the phase coils of the rotor winding on the sliding of the ISEM experimental sample

Taking into account the conditions of dynamic adaptation of the parameters of the spatial elements of the active part of the ISEM during the transition from 3D to 2D field modeling. The three-dimensional domain of the frontal parts of the armature windings and ISEM rotor can be represented as active and inductive elements of an electric circuit. Figure 8 shows the principle of the structure of the circuit-field model, where the slot parts of the armature and rotor windings, which are elements of the geometric calculation domain of the active part of the ISEM field model ($\Omega 1$ – subdomain of the armature core; $\Omega 2$ – subdomain of the upper and lower layers of the slot part of the armature winding; $\Omega 3$ – subdomain of the rotor core; $\Omega 4$ – subdomain of the slot part of the rotor winding), connected respectively to the frontal parts of the armature and rotor windings, which are represented by elements of electric circuits: mutual inductance between the frontal and slot parts of the armature winding section M^s_{nm}, which takes into account the edge effect regarding the magnetization of the end zone of the armature core by the frontal parts of the winding; the active resistance of the frontal part of the section R_{ls}; the total inductance of the front part of the winding section L_{ls}. For rotor winding sections – M^r_{nm}, R_{lr}, L_{lr}, respectively. The active resistance R_{lr} and the total inductance L_{lr} are presented as a function of the slip s.

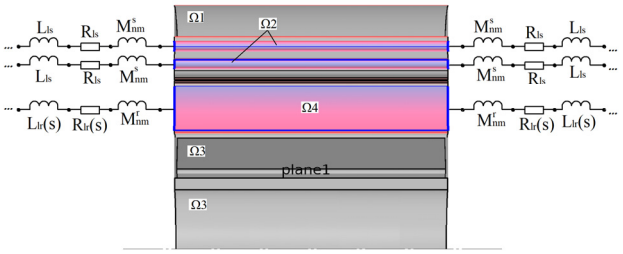

Fig. 8. *yz* cross-sectional plane of the active part of ISEM showing the frontal parts of the sections of the armature windings and rotor as elements of an electric circuit

The combination of the frontal and slot parts of the section of the armature windings and the rotor (i.e., the electric circuit with the spatial subdomain of the

geometric model) can also be performed, for example, with the help of «External I vs. U» terminals when combining «Rotating Machinery, Magnetic» and «Electrical Circuit» interfaces in the structure of COMSOL Multiphysics tools.

After the edge effects were taken into account, as well as the change in the active resistance and inductance of the front parts of the rotor winding due to ISEM sliding, it is reasonable to switch from the spatial to the plane-parallel formulation of the electromagnetic field distribution. At the same time, the spatial slot active part of ISEM can be represented as its projection in the *xy*-plane at a given equivalent depth L_z of the calculation area [10, 12, 14]:

$$\begin{cases} \boldsymbol{A}_{i,j} = L_z \cdot A_{z\,i,j}; \quad \boldsymbol{B}_{i,j} = \boldsymbol{i} \cdot B_{x\,i,j} + \boldsymbol{j} \cdot B_{y\,i,j}; \\ \boldsymbol{H}_{i,j} = \boldsymbol{i} \cdot H_{x\,i,j} + \boldsymbol{j} \cdot H_{y\,i,j}; \overline{B}_{x\,i,j} = -\dfrac{\partial \overline{A}_{i,j}}{\partial x}; \\ \overline{B}_{y\,i,j} = -\dfrac{\partial \overline{A}_{i,j}}{\partial y}; \overline{H}_{x\,i,j} = \dfrac{\overline{B}_{x\,i,j}}{\mu_{i,j}}; \overline{H}_{y\,i,j} = \dfrac{\overline{B}_{y\,i,j}}{\mu_{i,j}}. \end{cases} \tag{35}$$

This reduction of the geometric dimension allows us to use flat triangular elements of the calculation mesh and significantly increase the efficiency of the numerical implementation. In this case, the electromagnetic field description model for transient operating modes will correspond to (1), and the gauge condition is automatically fulfilled.

Thus, the adapted 2D circuit-field model of an induction-synchronous electromechanical converter can be represented as shown in Fig. 9, where the solid lines show the electrical connection of the ISEM armature winding inputs to the power cells, and the dashed lines show the electrical connection of the armature winding terminals, which form two independent «stars», which are connected according to the anode and cathode groups of the rectifier (the connection of the front and slot parts of the sections, as well as the coils in the coil groups of the armature winding is not shown in Fig. 9).

In order to carry out an ISEM study in the modes of non-operation and under load, the equations of the transient electromagnetic field must be supplemented with a system of equations of the angular speed of the rotor and the electromagnetic torque [26, 27]:

$$\begin{cases} \dfrac{\mathrm{d}\omega_m}{\mathrm{d}t} = \dfrac{M_e - M_c}{J}; \\ \dfrac{\mathrm{d}\phi}{\mathrm{d}t} = \omega_m; \\ M_e^{\,ave} = \dfrac{1}{R_o - R_i} \cdot \dfrac{L_z}{\mu_0} \int\limits_{S_{ag}} B_r B_\varphi r \mathrm{d}S_{ag}, \end{cases} \tag{36}$$

where M_e is the electromagnetic torque, N·m; M_c is the load moment, N·m; J is the moment of inertia of the rotor, kg·m^2; ω_m is the rotor angular speed, rad/s; φ is the rotor position angle, rad; r is the outer radius of the rotor core, m; L_z is the length of the armature and rotor package, m; B_r, B_φ are the radial and azimuthal components of magnetic flux density, T; R_o is the outer radius of the air gap, m; R_i is the inner radius of the air gap, m; S_{ag} is the cross-sectional area of the air gap, m^2.

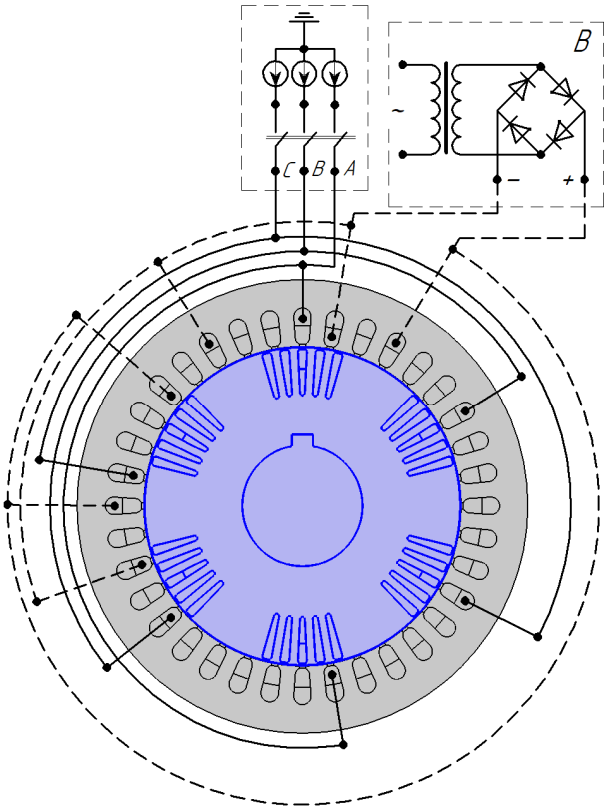

Fig. 9. Schematic-geometric interpretation of the adapted 2D circuit-field model of ISEM

Thus, an adapted dynamic 2D circuit-field model of ISEM was developed, which with high accuracy and efficiency of numerical implementation allows for transient modes of operation to take into account interconnected electromagnetic and mechanical processes, taking into account both design features and schematic implementation of the winding system, nonlinearity of magnetic and electrophysical properties of active materials, skin and edge effects of the end zones of the active part, as well as changes in the active resistance and inductance of the front parts of the rotor windings depending on its sliding in the transient and quasi-transient modes of its operation.

Experimental study of the ISEM test sample. In order to confirm the adequacy of the studied electromagnetic and mechanical processes and the accuracy of numerical calculations based on the proposed adapted 2D circuit-field model, physical tests of the ISEM experimental sample (Fig. 10) in the short-circuit and non-operation modes were carried out in the laboratory conditions of National University «Zaporizhzhia Polytechnic». The experimental ISEM sample itself is shown in Fig. 11. Currents in the phases of the armature winding, as well as in its parallel branches, were measured using an oscilloscope type OWON XDS3202E.

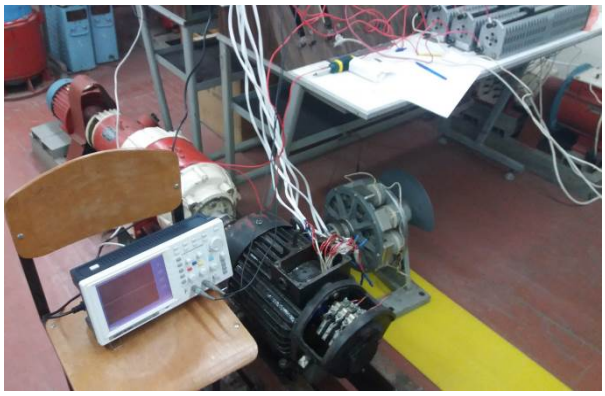

Fig. 10. Experimental stand of the ISEM test sample

a *b*

Fig. 11. Active part of the armature (*a*) and rotor (*b*) of the ISEM experimental sample

Table 2 shows the results of data validation of 3D and 2D circuit-field modeling and physical testing according to phase currents with simultaneous supply of the phases of the armature winding *A*, *B*, *C*, and ISEM excitation current in the short-circuit mode. When measuring the excitation current, the phase inputs of the armature winding were disconnected from the network. DC voltage from the excitation system was applied alternately to each phase *A*, *B*, *C* with the terminals of the winding phases open, forming two separate «stars» (points «0–» and «0+»), and immediately behind all phases of the armature winding at connecting the winding terminals into separate «stars». As the analysis of experimental data (Table 2) shows, the current discrepancy for the 3D circuit-field model does not exceed 3.45 %, and for the 2D adapted circuit-field model – 4.34 %, which confirms the high efficiency of the proposed methods of dynamic adaptation of complex spatial elements of the active part of ISEM, as well as the high accuracy of the numerical calculation of the 3D circuit-field model itself. The most difficult task in the development of a 3D spatial geometric model (not only ISEM, but also any EM) is the implementation of a symmetrical arrangement of the coils of the armature winding (rotor) among themselves, as well as the movement of their frontal parts. This is further complicated when the armature winding is two-layered, that is, the left part of the section is placed in the lower layer of the slot, and the right part of the section is placed in the upper one. To confirm the condition of symmetrical placement of the armature winding coils of the ISEM 3D geometric model, there is a measurement of the ohmic resistance in each phase. At the same time, the resistance of each phase coil group must be the same. Thus, the validation of ohmic resistance data in each of the phases was carried out using 3D numerical modeling and an adapted 2D circuit-field model as well as the results of measuring the ohmic resistance of the phases of the armature winding of the ISEM experimental sample. According to the results of numerical calculation and actual measurement, the discrepancy by ohmic resistance of phases *A*, *B*, *C* of the ISEM armature winding does not exceed $\delta R_a \leq 0.00694$ %.

Table 3 shows the results of the validation of 2D circle-field modeling and physical testing based on the available spectra of harmonics (k = 1,2,3,6,7) of the phase currents of the armature *A*, *B*, *C*, in the non-operation mode at the excitation current $I_f = 0$. Experimental oscillograms of ISEM phase currents are shown in Fig. 12.

As the data analysis (Table 3) shows, the discrepancy of the fundamental harmonic current in numerical calculations based on the adapted 2D circuit-field model and the results of the experimental study of the experimental ISEM does not exceed 8.61 %. At the same time, the current spectra of the digital current signals of the experimental ISEM during the test fully correspond to the harmonic composition of the phase currents according to the adapted 2D circuit-field model, and also have a negligible value of discrepancy in the amplitude values of the current spectra of higher harmonics (2.06 % – 4.33 %).

Table 2

Validation of 3D and 2D circuit-field modeling and physical testing by phase currents and ISEM excitation current in the short-circuit mode

ISEM armature winding power suuply options	Discrepancy by current $\delta I_{a,i}\|_{A,B,C}$ and $\delta I_{f,i}\|_{A,B,C}$, %	
	by 3D circuit-field model	by 2D adapted circuit-field model
With simultaneous power supply of phases *A*, *B*, *C* without excitation current	3,18 – 3,45	3,96 – 4,34
Power supply with rectified current of phases *A*, *B*, *C* of the armature winding when opening zero points «0–» and «0+»	2,58 – 2,62	3,03 – 3,24
Power supply with excitation current of phases *A*, *B*, *C* of the armature winding at connecting the winding terminals into separate «stars» («0–» and «0+» points)	2,39 – 2,78	3,11 – 3,31

Table 3

Validation of data based on the spectra of phase currents of 2D circuit-field modeling and physical testing of the experimental ISEM in the non-operation mode without the presence of excitation current

	Discrepancy by amplitude values of phase current harmonics $\delta I_{a,i}\|_{A,B,C}$, $\delta I_{a,i}\|_{A1,B1,C1}$, $\delta I_{a,i}\|_{A2,B2,C2}$, %				
	k = 1	k = 2	k = 3	k = 6	k = 7
Armature current (phases *A*, *B*, *C*)	7,96 – 8,61	2,06 – 2,12	4,11 – 4,33	2,8 – 3,09	3,66 – 3,96
Armature current in the first parallel branch (phases *A*1, *B*1, *C*1)	7,38 – 7,98	2,54 – 2,62	4,18 – 4,27	2,18 – 2,25	3,22 – 3,81
Armature current in the second parallel branch (phases *A*2, *B*2, *C*2)	7,89 – 8,26	2,42 – 2,5	3,96 – 4,05	2,89 – 3,13	3,9 – 4,21

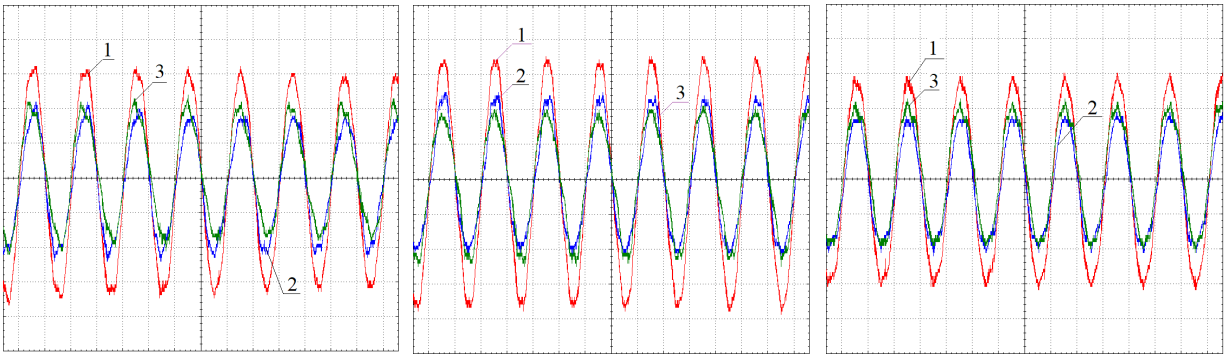

a *b* *c*

Fig. 12. Oscillograms of ISEM armature currents in the non-operation mode in the absence of excitation current:
a) 1 – armature current of phase *A*, 2 – phase *A*1 current (branch 1), 3 – phase *A*2 current (branch 2);
b) 1 – armature current of phase *B*, 2 – phase *B*1 current (branch 1), 3 – phase *B*1 current (branch 2);
c) 1 – armature current of phase *C*, 2 – phase *C*1 current (branch 1), 3 – phase *C2* current (branch 2)

Thus, the high efficiency and accuracy of the numerical implementation of the mathematical adapted 2D circuit-field model of ISEM in the non-operation mode are confirmed, as well as the convergence of the reproduction of the armature phase current curves. In addition, according to the obtained data of current discrepancies of the experimental ISEM, the high accuracy and efficiency of the proposed methods of decomposition and dynamic synthesis are confirmed, as well as the methodology for determining the active resistances and inductance of the end parts of the windings depending on the ISEM rotor slip, which provides the conditions for dynamic adaptation of 3D-2D circuit-field model of ISEM

Conclusions.

1. Based on the developed 3D circuit-field model of transient electromagnetic processes of the ISEM experimental sample, a decomposition method is proposed, which consists in separating its multi-component spatial structure into several separate subdomains (calculation zones): the core and the slot part of the armature winding; the left and right front parts of the armature winding; core and slot part of the rotor winding; respectively, the left and right front parts of the phase coils of the rotor winding.

2. A method of dynamic synthesis is proposed with adaptation of the conditions for combining electromagnetic parameters at the boundaries of the calculation subdomains of the frontal and slot parts of the armature and rotor windings of ISEM, which allows to match the flow of electromagnetic processes in the decomposed subdomains of ISEM to the electromagnetic processes in its integral calculation domain.

3. On the basis of the proposed methods, the share of the magnetic field energy determined by the action of edge effects in the end zones of the ISEM is determined. For problems of adaptation of 3D to 2D numerical calculations, it is proposed to take it into account through mutual inductance when replacing the spatial elements of the frontal parts of the armature winding with elements of the electric circuit.

4. For separate calculation subdomains of the frontal parts of the armature and ISEM rotor windings, when applying the variational formulation of the electromagnetic field equations taking into account the movement of the frontal parts of the ISEM rotor winding, the dependence of the active resistance and inductance of the frontal parts of the armature and rotor on the ISEM rotor slip has been determined.

5. Based on the developed methods, a new principle of the structure of the 2D circuit-field ISEM model is proposed, which consists in the fact that the slot parts of the armature and rotor windings are elements of the geometric calculation domain of the active part of the ISEM field model, and the frontal parts of the armature and rotor windings are represented by elements of electric circuit.

6. Due to the validation of the results of the numerical calculation with the data of the experimental study of the ISEM test sample, the high efficiency of the proposed methods of decomposition and dynamic synthesis and the accuracy of the numerical implementation of 3D and 2D circuit-field models of the ISEM have been confirmed. In the short-circuit mode, the discrepancy by armature current for the 3D circuit-field model does not exceed 3.45 %. For the adapted 2D circuit-field model – 4.34 %. In the non-operation mode, the discrepancy by the armature current of the main harmonic in numerical calculations based on the adapted 2D circuit-field model and the results of the ISEM experimental study does not exceed 8.61 %.

7. The proposed methods can be used for different types of electric machines.

Conflict of interest. The author declares no conflict of interest.

REFERENCES

1. Lushchyk V.D., Ivanenko V.S. Multipole cascade synchronous machines. *Electromechanical and Energy Saving Systems*, 2011, no. 2, pp. 121-123. (Ukr).

2. Luschik V.D., Ivanenko V.S., Borzik V.L. Synchronous cascade engine with combined winding. *Electrical Engineering & Electromechanics*, 2011, no. 1, pp. 31-32. (Ukr).

3. Lushchyk V.D., Semenov V.V. A new type of low-speed asynchronous-synchronous motor. *Coal of Ukraine*, 2008, no. 9, pp. 39-41. (Ukr).

4. Lushchyk V. D. *Prospective Directions for Improving Electric Machines*. Kyiv, Myronivska drukarnia Publ., 2015 264 p. (Ukr).

5. Kopylov Y.P. *Mathematical Modeling of Electrical Machines*. Moscow, Vysshaia Shkola Publ., 2001. 327 p. (Rus).

6. Lozynskyi A.O., Moroz V.I., *Paranchuk Ya.S. Solving Electromechanics Problems in MathCAD and MATLAB Environments*. Lviv, Mahnoliia Publ., 2007. 215 p. (Ukr).

7. Rohozyn H.H. *Determination of Electromagnetic Parameters of AC Machines. New Experimental Methods*. Kyiv, Tekhnika Publ., 1992. 168 p. (Ukr).

8. Amiri E. Circuit modeling of double-armature rotary-linear induction motor. *IECON 2014 - 40th Annual Conference of the IEEE Industrial Electronics Society*, 2014, pp. 431-436. doi: https://doi.org/10.1109/IECON.2014.7048536.
9. Semenova M.N., Yakushev I.A., Vasilyeva A.V., Sabychikova A.A., Monastyrev A.K., Kazazaeva D.V. Computer Modeling of DC and AC Motor Systems by Different Methods and Determination of Errors them. *2022 4th International Conference on Control Systems, Mathematical Modeling, Automation and Energy Efficiency (SUMMA)*, 2022, pp. 711-715. doi: https://doi.org/10.1109/SUMMA57301.2022.9973896.
10. Andrzej D. Finite element modeling of magnetic field in electrical machines: Scalar or vector potential formulation part I: Comparative description of methods. *2016 13th Selected Issues of Electrical Engineering and Electronics (WZEE)*, 2016, pp. 1-6. doi: https://doi.org/10.1109/WZEE.2016.7800208.
11. Zhang B., Wu F., Zhang Z., Wei Z., Xi J. 3D Magnetic Field Finite Element Analysis of Dual-Stator PM Spherical Motor. *2019 Chinese Control And Decision Conference (CCDC)*, 2019, pp. 5616-5620. doi: https://doi.org/10.1109/CCDC.2019.8832404.
12. Ferkova Z. Comparison of two-phase induction motor modeling in ANSYS Maxwell 2D and 3D program. *2014 ELEKTRO*, 2014, pp. 279-284. doi: https://doi.org/10.1109/ELEKTRO.2014.6848902.
13. Vaskovskyi Y.M., Tsivinskiy S.S. Three dimensional mathematical model of electromagnetic processes in the end zone of the turbogenerator rotor. *Technical Electrodynamics*, 2016, no. 1, pp. 34-39. (Ukr). doi: https://doi.org/10.15407/techned2016.01.034.
14. Fireteanu V., Constantin A.-I., Zorig A. Finite Element 2D and 3D Models of a Rotor Bar Breakage in a Squirrel-Cage Induction Motor. *2019 IEEE Workshop on Electrical Machines Design, Control and Diagnosis (WEMDCD)*, 2019, pp. 157-162. doi: https://doi.org/10.1109/WEMDCD.2019.8887801.
15. Yarymbash D., Kotsur M., Subbotin S., Oliinyk A. A new simulation approach of the electromagnetic fields in electrical machines. *2017 International Conference on Information and Digital Technologies (IDT)*, 2017, pp. 429-434. doi: https://doi.org/10.1109/DT.2017.8024332.
16. Kotsur M., Yarymbash D., Yarymbash S., Kotsur I. A new approach of the induction motor parameters determination in short-circuit mode by 3D electromagnetic field simulation. *2017 IEEE International Young Scientists Forum on Applied Physics and Engineering (YSF)*, 2017, pp. 207-210. doi: https://doi.org/10.1109/YSF.2017.8126620.
17. Milykh V.I., Tymin M.G. A comparative analysis of the parameters of a rotating magnetic field inductor when using concentric and loop windings. *Electrical Engineering & Electromechanics*, 2021, no. 4, pp. 12-18. doi: https://doi.org/10.20998/2074-272X.2021.4.02.
18. Milykh V.I. Numerical-field analysis of active and reactive winding parameters and mechanical characteristics of a squirrel-cage induction motor. *Electrical Engineering & Electromechanics*, 2023, no. 4, pp. 3-13. doi: https://doi.org/10.20998/2074-272X.2023.4.01.
19. Vaskovskyi J.M., Haydenko J.A. Research of electromagnetic processes in permanent magnet synchronous motors based on a «electric circuit - magnetic field» mathematical model. *Technical Electrodynamics*, 2018, no. 2, pp. 47-54. doi: https://doi.org/10.15407/techned2018.02.047.
20. Yarymbash D., Yarymbash S., Kotsur M., Divchuk T. Enhancing the effectiveness of calculation of parameters for short circuit of three-phase transformers using field simulation methods. *Eastern-European Journal of Enterprise Technologies*, 2018, vol. 4, no. 5(94), pp. 22-28. doi: https://doi.org/10.15587/1729-4061.2018.140236.
21. Kotsur M., Yarymbash D., Kotsur I., Yarymbash S. Improving efficiency in determining the inductance for the active part of an electric machine's armature by methods of field modeling. *Eastern-European Journal of Enterprise Technologies*, 2019, vol. 6, no. 5(102), pp. 39-47. doi: https://doi.org/10.15587/1729-4061.2019.185136.
22. Bellman R., Dreyfus S. *Applied Dynamic Programming*. Princeton University Press, New Jersey, 1962. 363 p.
23. Raviart P.A. Pseudo-viscosity methods and nonlinear hyperbolic equations. *Proceedings of the Royal Society of London. A. Mathematical and Physical Sciences*, 1971, vol. 323, no. 1553, pp. 277-283. doi: https://doi.org/10.1098/rspa.1971.0104.
24. Landau L.D., Lifshyts E.M. *Theoretical physics. Vol. 2. Field Theory*. Moscow, Nauka Publ., 1988. 59 p. (Rus).
25. Silvester P.P., Ferrari R. L. *Finite Elements for Electrical Engineers*. Cambridge University Press, 1990. 425 p.
26. Sadowski N., Lefevre Y., Lajoie-Mazenc M., Cros J. Finite element torque calculation in electrical machines while considering the movement. *IEEE Transactions on Magnetics*, 1992, vol. 28, no. 2, pp. 1410-1413. doi: https://doi.org/10.1109/20.123957.
27. Skalka M., Ondrusek C., Schreier L., Michailidis P. Torque components identification of induction machine by FEM. *International Aegean Conference on Electrical Machines and Power Electronics and Electromotion, Joint Conference*, 2011, pp. 185-189. doi: https://doi.org/10.1109/ACEMP.2011.6490592.

Received 27.01.2024
Accepted 09.03.2024
Published 20.06.2024

M.I. Kotsur[1]*, PhD, Assistant Professor,*
[1] National University «Zaporizhzhia Polytechnic»,
64, Zhykovskii Str., Zaporizhzhia, 69063, Ukraine,
e-mail: kotsur_m@ukr.net (Corresponding Author)

How to cite this article:
Kotsur M.I. Development of methods for adapting the parameters of spatial end winding sections in 2D circuit-field models of induction-synchronous electric machines. *Electrical Engineering & Electromechanics*, 2024, no. 4, pp. 9-21. doi: https://doi.org/10.20998/2074-272X.2024.4.02